Research Article

Influence of liquid nitrogen on residual circumferential distortion, weld penetration and delta-ferrite distribution in clamped tungsten inert gas welded butt joint of 316 stainless steel

Muhammad Asim Azeem[1] · Zia Ullah Arif[2] · Masood Shah[1] · Ehtsham ur Rehman[2,3] · Ali Tariq[4]

Received: 18 May 2020 / Accepted: 27 August 2020 / Published online: 7 September 2020

Abstract
AISI 316 stainless steel (SS316) is an attractive material for industrial applications. Welding of this alloy can lead to severe distortion that often results in dimensional inaccuracies. With the help of specially designed fixture and clamping mandrels, tungsten inert gas (TIG) welding on SS316 pipes is employed to investigate the effect of liquid nitrogen on the circumferential distortion, weld penetration and delta-ferrite distribution in different welding zones. The experimental results reveal that the presence of trailing heat sink in TIG welded butt joint has almost zero distortion at a distance of 30 mm from the weld centerline and 64% decrement in residual circumferential distortion at the center of the weld bead. A metallurgical microscope is used to find the weld penetration, (fusion zone) FZ and (heat affected zone) HAZ. The results illustrate that increase in current and the presence of intensive cooling media yield deeper penetration in TIG welding. Liquid nitrogen (LN_2) also constricts the FZ and HAZ. Instead of evaluating delta-ferrite contents using the ferrite number technique, a MATLAB® code for image processing is developed to evaluate the delta-ferrite distribution in the different regions of a single-pass weldment. Delta-ferrite contents are maximum in the presence of intensive cooling media near HAZ and increase with an increase in the current value. Hence, TIG welding with LN_2 as trailing heat sink is the most suitable scheme to weld industrial pipes owing to its higher weld penetration, higher delta-ferrite contents and minimum circumferential distortion.

Keywords TIG welding · Trailing heat sink · Liquid nitrogen · Circumferential distortion · Weld penetration · Delta-ferrite contents

Abbreviations

TIG	Tungsten Inert Gas
GTAW	Gas tungsten arc welding
SMAW	Shielded metal arc welding
GMAW	Gas metal arc welding
SS316	316 Stainless steel
LN_2	Liquid nitrogen
DC-LSND	Dynamically controlled low-stress non-distortion
VFD	Variable frequency drive
EDM	Electric discharge machine
FZ	Fusion zone
HAZ	Heat affected zone
BM	Base metal
V	Voltage
I	Current
S	Welding speed
η	Thermal efficiency (η = 0.6 for TIG welding according to European system EN ISO 1011–1)

✉ Zia Ullah Arif, zia_ul_arif@yahoo.com; chzia980@gmail.com; zia.arif@skt.umt.edu.pk | [1]Mechanical Engineering Department, University of Engineering and Technology, Taxila 47080, Pakistan. [2]Mechanical Engineering Department, University of Management and Technology, Lahore, Sialkot Campus 51041, Pakistan. [3]Mechanical Engineering Department, University of Engineering and Technology, Lahore, Pakistan. [4]School of Mechanical and Manufacturing Engineering, National University of Sciences and Technology, Islamabad, Pakistan.

SN Applied Sciences (2020) 2:1640 | https://doi.org/10.1007/s42452-020-03446-y

D_{AO} Average diameter of original pipe
D_{AW} Average diameter of welded pipe

1 Introduction

Industrial pipes play a pivotal role in several industrial sectors like oil, chemical, petrochemical and nuclear engineering fields. Pipes welding is a crucial technique that affects the service life of different joints. Welding is a localized heating technique that causes the expansion of the material followed by the localized contraction due to cooling. This localized expansion and contraction welcome the inherent property of welding that is the introduction of residual stresses [1]. Normally, gas tungsten arc welding (GTAW), shielded metal arc welding (SMAW) and gas metal arc welding (GMAW) are the main techniques to join pipes of small diameter and low thickness [2, 3]. The vicinity of girth-butt welded pipes contains radial shrinkage along with localized residual stresses. These stresses come into play due to uneven heating and cooling of specimens [4]. These stresses could be fatal for the integrity of the pipes because they expedite the intergranular stress corrosion cracking and fatigue cracking process. Phase transformation and alteration of material properties are the effects of welding along with the introduction of thermal stresses [5]. Residual stresses and distortions are detrimental to the strength and integrity of the welded structures. Due to this reason, influencing parameters such as current, voltage, welding speed, etc. must be considered [6, 7] and controlled to mitigate the residual distortion and residual stresses [8]. Different mechanical methods were applied to overcome the residual stresses and distortions but these techniques required extra efforts before or after the welding [9]. For instance, the most used technique to handle these stresses is post-weld heat treatment (PWHT) but it has high running and equipment cost, causes surface oxidation and it is more time consuming [10]. The material expands due to heat during welding and shrinks after cooling. This shrinkage under external constraint cause distortion and residual stresses. As previously reported by the researchers, this distortion is induced due to temperature change [11]. In order to counter this distortion, a change of temperature field can be a good option to follow. Keeping in view the temperature field, the concept of thermal tensioning for mitigating the residual stresses and distortions was introduced by Guan and his teammates in the 1980s [12]. After the development of low-stress non-distortion (LSND), Guan and his team further introduced a technique in which they added heat sink after the welding torch. This method of after cooling was very helpful in the reduction of residual stresses and distortions as imminent from the name, "Dynamically controlled low-stress non-distortion (DC-LSND) method" [13]. DC-LSND is a technique which comprises of intensive cooling source and the welding torch to mitigate the welding distortion and residual stresses [14]. Welding speed, current, distance between the welding arc and heat sink, type of heat sink and flow rate of the coolant are the major influencing parameters in the DC-LSND phenomenon [15]. Shen et al. [16] reported that for the DC-LSND effect to take place properly the welding speed must be low, the distance between the torch and heat sink must be small and the diameter of the jet must be so that the cooling effect can reach deep into the metal. Richards et al. and Xu et al. investigated that positioning and power of coolant have prime importance in controlling the distortion and the cooling capacity of liquid CO_2 is greater than water [17, 18]. Ji et al. [19] analyzed that by using LN_2 trailing cooling source in friction stir welding, the high temperature zone and plastic strains were reduced which mitigate the distortions and residual stresses as compared to the conventional welding techniques. Research on the cryogenic effect that has been occurred up till now is merely on thin welded metal sheets. Investigations on LN_2 effect as a trailing heat sink for piping are still unexplored by the engineers and researchers. This area needed to be discovered owing to its significance in industries, as piping is the most often used product manufactured by the steel industry [20]. Furthermore, a study on pipe welding is more vital because of its critical use in chemical, pharmaceutical, power plants, and oil and gas industries. So, there is a prime need for exploring this overlooked area in the study of cryogenic liquid using tungsten inert gas (TIG) welding on pipes. In this paper, an attempt has been made to explore this field of DC-LSND method for pipes. For this research purpose, a special fixture was designed to apply this technique to the cylindrical specimens. These specimens were welded by using this apparatus with and without trailing heat sink. Nitrogen gas has been used in heat sink instead of conventional heat sink gases like CO_2 (liquid and gas). Furthermore, the welding technique used for this process is TIG rather than SMAW or GMAW because former techniques cause more residual and thermal stresses at larger surface areas than the latter two. This is due to the reason that during TIG travel speed is always lower than GMAW and SMAW. So, TIG effects a larger surface area, producing more distortion in the vicinity of the weldment. Consequently, this effect can be studied more precisely. Welding distortions, penetration and delta-ferrite distribution of the specimens have been measured and their comparison has been made for a better understanding of the results.

The research article has been organized into the following sections. Section 1 presents the literature review and background knowledge about the effect of cryogenic liquid on different characteristics of the welding.

Table 1 Chemical composition and mechanical properties of AISI SS316

Material	Chemical Composition								Mechanical Properties		
	C	Mn	P	S	Si	Cr	Ni	Mo	Ultimate/MPa	Yield/MPa	Elongation/%
SS316 (Min–Max)	.08	2.0	.045	.03	1.0	16–18	11–14	2–3	515	205	35
SS316 (Actual)	.073	1.28	0.03	.001	0.4	16.5	10	2.02	495	175	37

Table 2 Summary of welding technique and its fixed parameters

Welding type	Autogenous TIG welding
Welded material	AISI 316 stainless steel
Weld groove	No groove preparation
Number of passes	Single pass
Joint type	Butt joint
Arc length	2 mm
Welding speed	13 mm/s
Shielding gas	Pure argon (99.99%)
Welding direction	Circumferential (clockwise)
Flow rate of LN_2	200 ml/min
Tip angle of the tungsten electrode	15°
Angle between welding electrode and welding tip	45°

Section 2 contains a brief overview of SS316, experimental setup, sample preparation for microscopic analysis and technique used for calculating residual distortion. Section 3 includes detailed discussions and results about the residual circumferential distortion, weld penetration and distribution of delta ferrite contents. Finally, the conclusions are drawn in Sect. 4.

2 Experimental procedure

2.1 Materials

AISI 316 stainless steel (SS316) pipe of nominal diameter 50 mm and schedule 10 was used in this study. Pipe length of one meter was procured from the Lianzhong stainless steel corporation, manufactured in China. The chemical composition (exact and as-received) [21] and mechanical properties [22] of base metal (BM) are presented in Table 1.

2.2 Welding technique and variables

The significant welding specifications and conditions employed in this experiment are given in Table 2. Original pipe length was cut into twenty-four pieces of 40 mm each. Two parts of 40 mm length were welded to produce twelve specimens. These twelve butt-welded joint samples were categorized into three groups named A, B and C as summarized in Table 3. Each group comprising of four samples. Table 3 also gives a complete description of the welding parameters.

Two parts of the specimen to be welded were mounted on a mandrel as shown in Fig. 1 Detailed view of the jig, clamping mandrels and pipe fixed on the

Table 3 Welding parameters and weld dimensions

Samples	Groups		Current (A)	Voltage (V)	Heat input (kJ/mm)	Weld size (mm		Circumferential distortion at centerline (μm)	Weld depth (μm
						FZ	HAZ		
1	A	Conventional TIG welding	165	29	0.221	4.14	3.94	0.55	1031
2			80	16	0.059	3.94	3.28	0.44	457.8
3			100	19	0.088	3.99	3.42	0.47	753.3
4			120	22	0.122	4.06	3.58	0.49	796.3
5	B	LN_2 as trailing heat sink	165	29	0.221	2.82	2.14	0.25	1327
6			120	22	0.122	2.72	1.89	0.23	939.9
7			100	19	0.088	2.64	1.76	0.22	862.8
8			80	16	0.059	2.52	1.46	0.20	485.8
9	C	Pre-cooling of specimens prior to the welding	165	29	0.221	3.26	2.92	0.33	1092
10			120	22	0.122	3.24	2.72	0.31	888.8
11			100	19	0.088	3.14	2.68	0.295	768
12			80	16	0.059	3.02	2.66	0.27	444.1

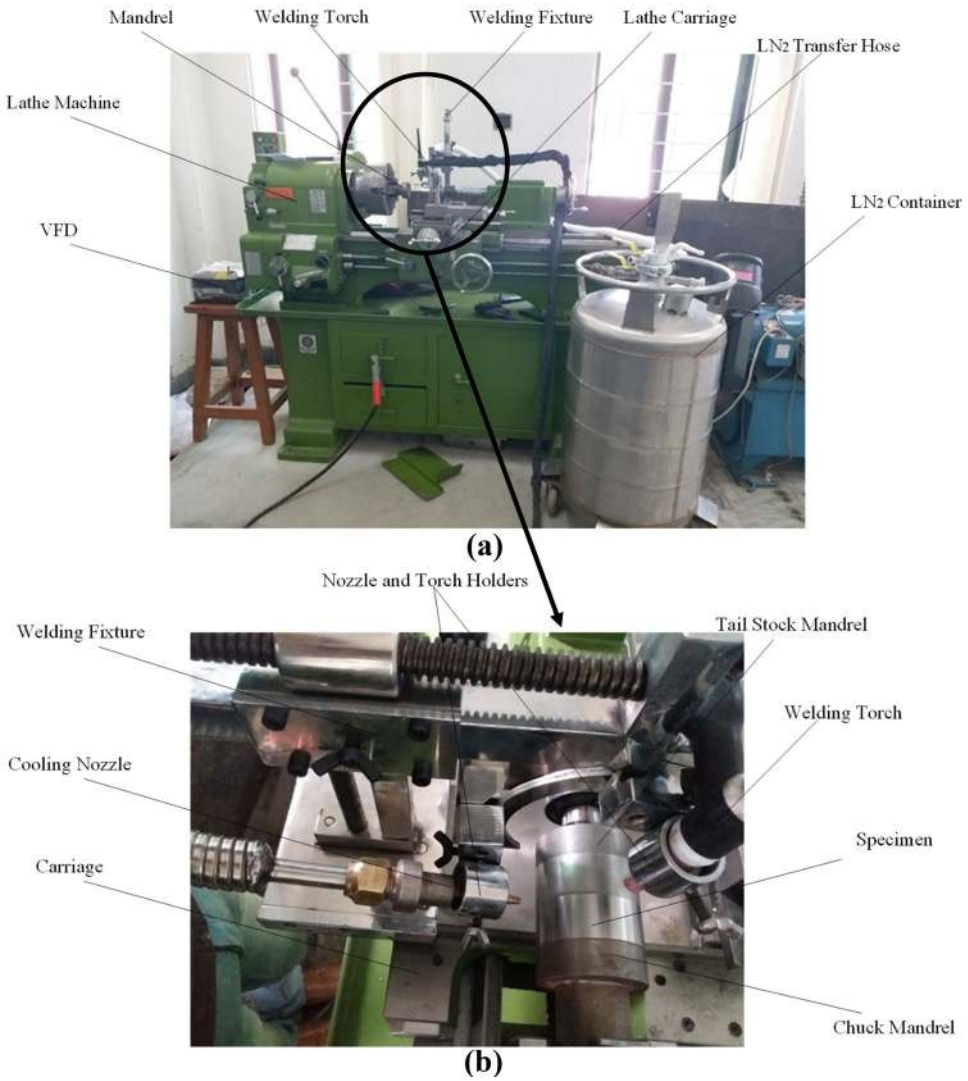

Fig. 1 **a** Experimental setup with trailing heat sink (liquid nitrogen). **b** Detailed view of Jig and clamping mandrels

lathe machine is shown in Fig. 1b. The speed of the lathe machine was controlled by the variable frequency drive (VFD) by varying the frequency of the input power supply. The mandrel (clamping device) was held and rotated at a constant speed by the chuck of the lathe machine and supported by the tailstock to avoid any relative motion between two parts. The TIG welding machine (Model T375) by Lincoln Electric has been used to perform single-pass autogenous TIG welding. TIG pencil-type welding torch of model TA-9P has been used along with this machine. Tungsten electrode of size 0.50 and Ceramic cup of number 3 is the specification of welding torch parts. The cooling nozzle used LN_2 as a trailing heat sink and welding torch was fixed on the specially designed jig in such a way that both were radially directed and focused towards the pipe joint. Jig permits the motion of both the cooling nozzle and the welding torch in three axes. Thus, allowing the variation in distance between nozzle and torch. During welding, a fixed distance of 40 mm was maintained between the cooling nozzle and the welding arc. As described previously by Sung et al. [4], this was the least possible distance between welding torch and cooling nozzle that is necessary to avoid the interference of the trailing heat sink with the welding arc. Specimens from three groups A, B and C were treated differently. In group A, no trailing heat sink was provided, merely TIG welding was done using the apparatus. In group B trailing heat sink was provided in addition to current variation. Moreover, in group C pre-cooling of the specimens for two minutes was done prior to the welding. Finally, the cross-sections of the TIG-welded specimens with or without LN_2 are shown in Fig. 2. Moreover, the heat input (kJ/mm) was calculated [23] by using the following Eq. (1)

$$\text{Heat input} = \frac{V \times I \times \eta}{S \times 1000}. \quad (1)$$

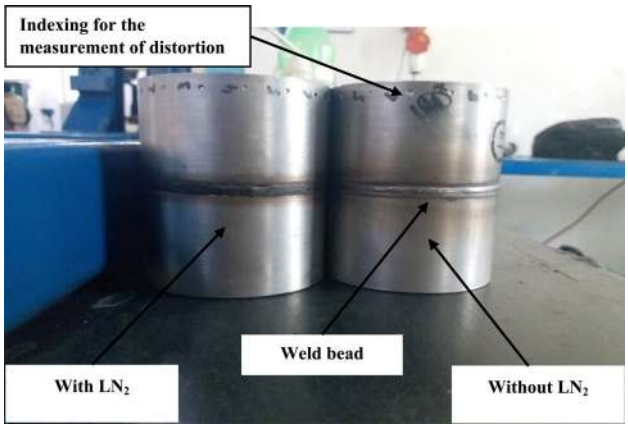

Fig. 2 Cross section of TIG-welded specimens with and without trailing heat sink

2.3 Measurement of circumferential distortion

All the specimens were equally divided circumferentially into 16 divisions at an angle of 22.5° by using indexing head on milling machine as shown in Fig. 3a. These indexed points were used to draw straight lines along the length of the welded specimen by using a lathe machine. The lines were drawn at a distance of 5 mm and 30 mm from the centerline of the weld bead to both sides of the specimen as depicted in Fig. 3b. Marking in such a manner gave us sixteen points on each circumferential line. These points were grouped into two sets of eight divisions. After this marking diameter was measured between the two marked points by using Mitutoyo micrometer (MDH-25 MB) of 0.1 µm resolution. For instance, division 1 of the first set and division 1 of the second set, division 2 of the first set and division 2 of the second set, this sequence followed up to 8 divisions. The average was taken of these eight values and from the resulting value, the average diameter of the original was subtracted to find the circumferential distortion. This technique was previously adopted by Sattari et al. [24].

2.4 Metallography

Weld dimensions includes depth of the welded specimens, fusion zone (FZ) and heat-affected zone (HAZ) were measured using an optical microscope. The specimens were prepared to be viewed under the optical microscope. These samples were cut from the welded portion into dimensions of 20 mm × 10 mm by using wire cut electric discharge machine (EDM). After that, these specimens were embedded in epoxy and polished with emery paper

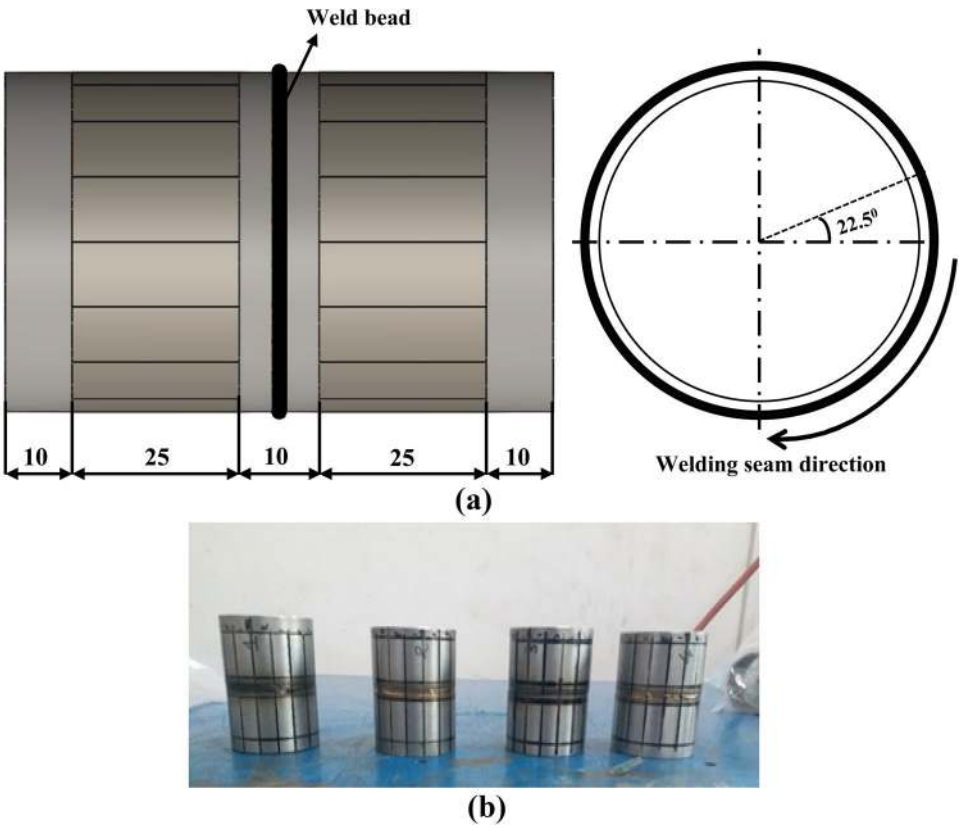

Fig. 3 **a** Configuration of weld bead on the circumference of SS316 pipe. **b** Marking of specimens to measure diametral distortion

from grades 120 to 4000 grits. Then, the specimens were creamed with the diamond crystal paste of 6 microns and 3 microns on a rotating polishing machine. As per ASM standards, all the specimens were electrolytically etched with the solution of 10% HCL in ethyl alcohol at 5 V for 3 min to reveal delta ferrite presence in SS316. An Olympus metallurgical microscope BX-51 was used to visualize these polished and scratch-free specimens. This microscope was equipped with image analyzer software to view the grain structure of welded specimens.

3 Results and discussions

The presence of LN_2 as a trailing heat sink in the TIG welding butt joint significantly affects the welding characteristics. The results of the testing were categorized into three groups.

(1) Residual circumferential distortion measurement
(2) Weld penetration depth measurement
(3) Delta-ferrite contents measurement

3.1 Circumferential distortion measurement

In this experiment, distortion can be termed as diametral or circumferential shrinkage. Diametral shrinkage was found by using Eq. (4) subtracting the mean diameter of the original pipe from the average value of the mean diameter of the welded pipe. The diameter of the specimen without welding was 62.06 mm. To find the distortion at every point, the average diameter of the pipe at that point after welding was found by taking an average of 8 points around the circumference and then subtracting it from the diameter of the specimen. Formulae to find out distortion are given in Eq. (2) to Eq. (4).

$$D_A W = \frac{DW1 + DW2 + DW3 + DW4 + DW5 + DW6 + DW7 + DW8}{8} \quad (2)$$

$$D_A O = \frac{DO1 + DO2 + DO3 + DO4 + DO5 + DO6 + DO7 + DO8}{8} \quad (3)$$

$$\text{Circumferential distortion} = \left|D_{AW} - D_{AO}\right| \quad (4)$$

D_{AO} was measured as 62.06 mm, it remained the same for all the specimens but D_{AW} for all the specimens was calculated after measuring the diameters of post welded specimens at eight different sets of points. Variations of circumferential distortion were shown by graphs to evaluate the influence of different parameters on the distortion.

3.1.1 Circumferential distortion with autogenous TIG welding

Figure 4 shows the variation of the diametral distortion with the increase in the current when no trailing heat sink was applied. Circumferential distortion increased as the current increased without application of the trailing heat sink. Shrinkage is maximum at the center of the weld and decreases towards the outer edges of the pipe for all the currents. The increase in current results in an increase in weld bead width as shown in Fig. 7. This increase in bead width would result in an increase in distortion due to high shrinkage at the weld sides. In addition to this, Prasad et al. [25] found that plastic strain induced due to variation of temperature during welding is the main cause of distortion. During cooling phase, SS316 shrinks and generates

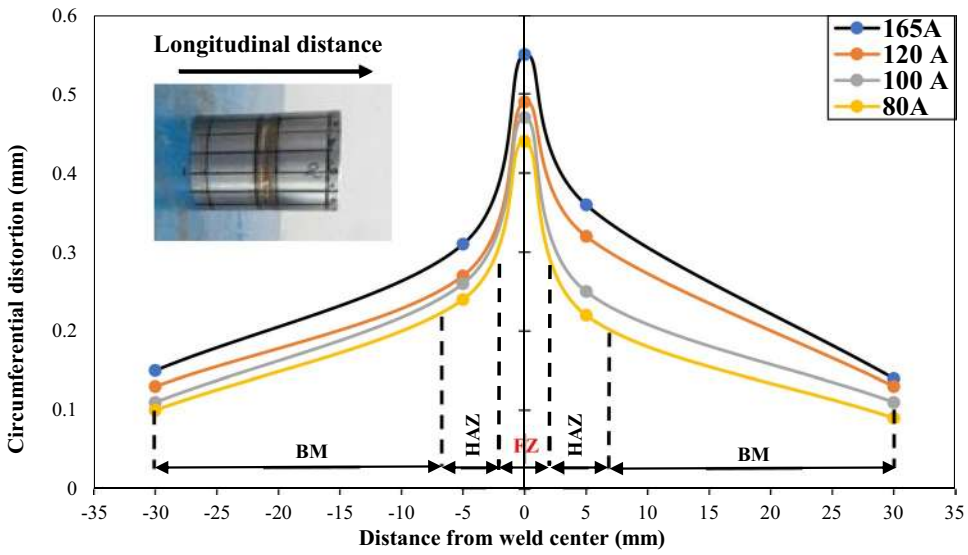

Fig. 4 Effect of current variation on residual distortion with autogenous TIG welding

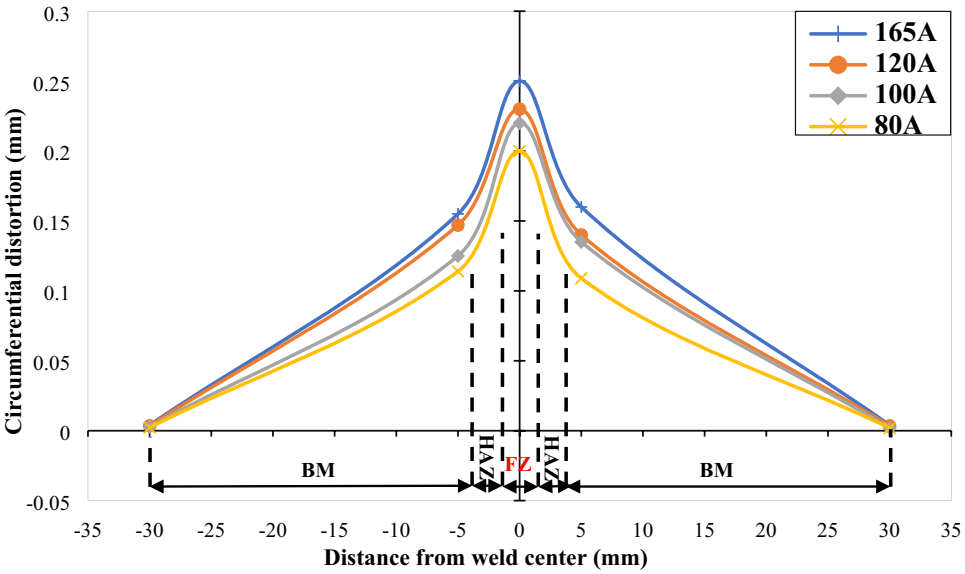

Fig. 5 Influence of current variation on residual distortion with liquid nitrogen

residual compressive stresses at the outer side and tensile stresses inside the pipe that caused the distortion. Moreover, with the increase in current value, the residual stresses spread to a wider range. These illustrations present a better explanation of the increase in the distortion with the increase in current.

3.1.2 Circumferential distortion with LN_2

In this case, the trailing heat sink was provided with the welding arc. Figure 5 illustrates the variation of the diametral distortion for different values of current. In Fig. 5 the distortions are shown at five different positions for each specimen. One point is at the center of the weldment and the other is at 5 mm and 30 mm on each side of the weld bead. Figure 5 depicts that TIG-welded specimens with trailing heat sink show the same trend as without trailing heat sink but SS316 weld specimens marked a significant reduction in circumferential distortion at the centerline of the weld due to the presence of an intensive cooling medium and almost becomes zero at the outer sides of the pipe. The maximum distortion around the weld vicinity with trailing heat sink is only 0.25 mm at 165 A. As stated by Quan et al. [26] that low temperature zone is formed due to the trailing heat sink which not only leads to the reduction of peak temperature and bead width but also shrinks high temperature zone. As a result, circumferential distortion is reduced. Furthermore, circumferential distortion mitigation also depends upon the heat transfer coefficient of the heat sink. The temperature of the specimens falls rapidly if the heat transfer coefficient of the heat sink is larger as in the case of LN_2. Consequently, temperature

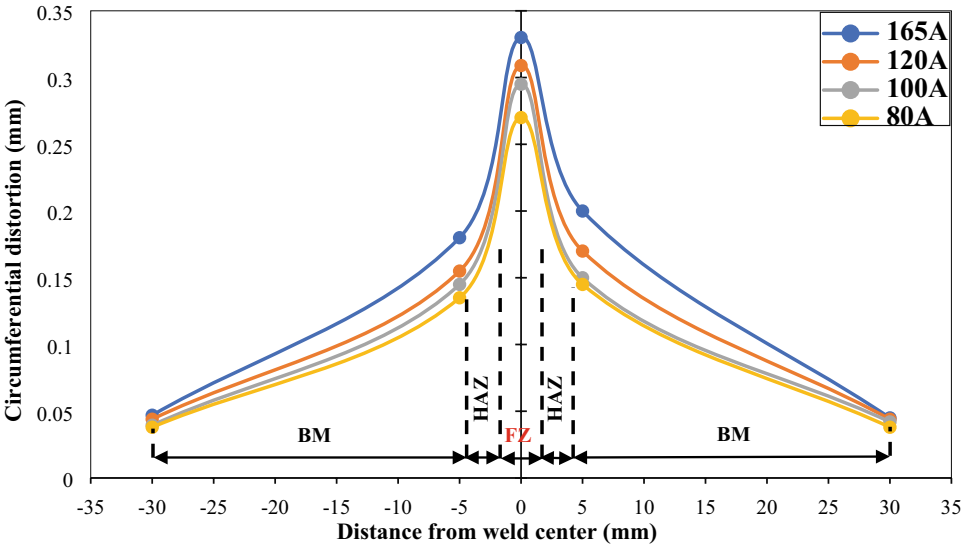

Fig. 6 Effect of current variation on residual distortion with pre-cooling

towards the sides of the weld falls significantly. In addition to this, clamping of specimens via mandrels also contributed in producing zero distortion at the ends in the presence of trailing heat sink and resulted in minimum the distortion towards the sides without intensive cooling media. Hence, it is proved [27, 28] that the clamping also plays a key role in mitigating residual distortion.

3.1.3 Circumferential distortion of pre-cooled (LN_2) specimens

Group C consists of specimens in which pre-cooling for two minutes was done prior to welding. In Fig. 6 circumferential distortions were compared for each value of current for pre-cooled specimens. As a result of this, circumferential distortion decreases as compared to conventional TIG-welded butt joints. But the influence of pre-cooling on distortion was less significant as compared to instantaneous cooling. It because pre-cooling results in rapid heat transfer [29] with the surrounding before welding that would keep on increasing the temperature of the cooled surface. As a result, it reduces lesser peak temperature upon welding. Hence, circumferential distortion is somewhat more than the trailing heat sink TIG-welded specimens (Fig. 7).

3.1.4 Comparison of circumferential distortion at different currents

Diametral distortions of the three different groups at each current value were compared to authenticate the technique that was more useful in the reduction of the diametral shrinkage. Fig. 8 depicts the distortion at centerline positions of welded specimens for all three cases. It is evident from the distortion values at different currents that the diametral shrinkage is reduced by the application of the trailing heat sink. The diametral shrinkages in welded pipes may occur due to the residual stresses induced during welding because of the expansion and contraction of the material under external constraint. By the application of the trailing heat sink, FZ and HAZ were constricted as summarized in Table 3. This constriction in weld dimensions is considered due to lower thermal cycles linked with trailing heat sink which decreased the temperature field in the weld section [15]. The tensile plastic strain may also come into play with the application of the intense cooling that balances the compressive strain induced due to the heating of the material during welding [19]. Figure 8a, b illustrate that the percentage reduction in circumferential distortion is more in the presence of intensive cooling media as compared to pre-cooled specimens.

3.2 Weld penetration depth

Weld penetration depths of the specimens were found by an optical metallurgical microscope across the cross-sectioned samples of the weld joints. Along the thickness of the pipe in the welding zone, the weld penetration was found by determining the thickness of the fused region while the remaining region appeared as a crack in which no fusion took place as shown in Fig. 9.

3.2.1 Weld penetration of the autogenous TIG welded specimens

Following Fig. 10a–d depict the weld penetration of the specimens welded without the application of trailing heat sink. Weld depths of these samples show an increasing trend with the increase in current. In this case, the maximum obtained weld penetration was 1.031 mm at 165 A as shown in Fig. 10a. When the current increases from 80

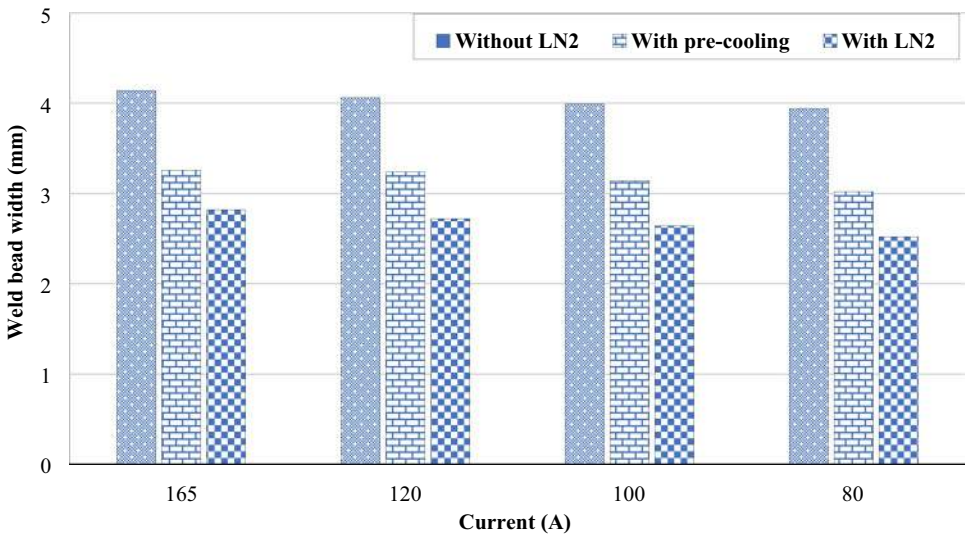

Fig. 7 The weld bead width under different cooling conditions

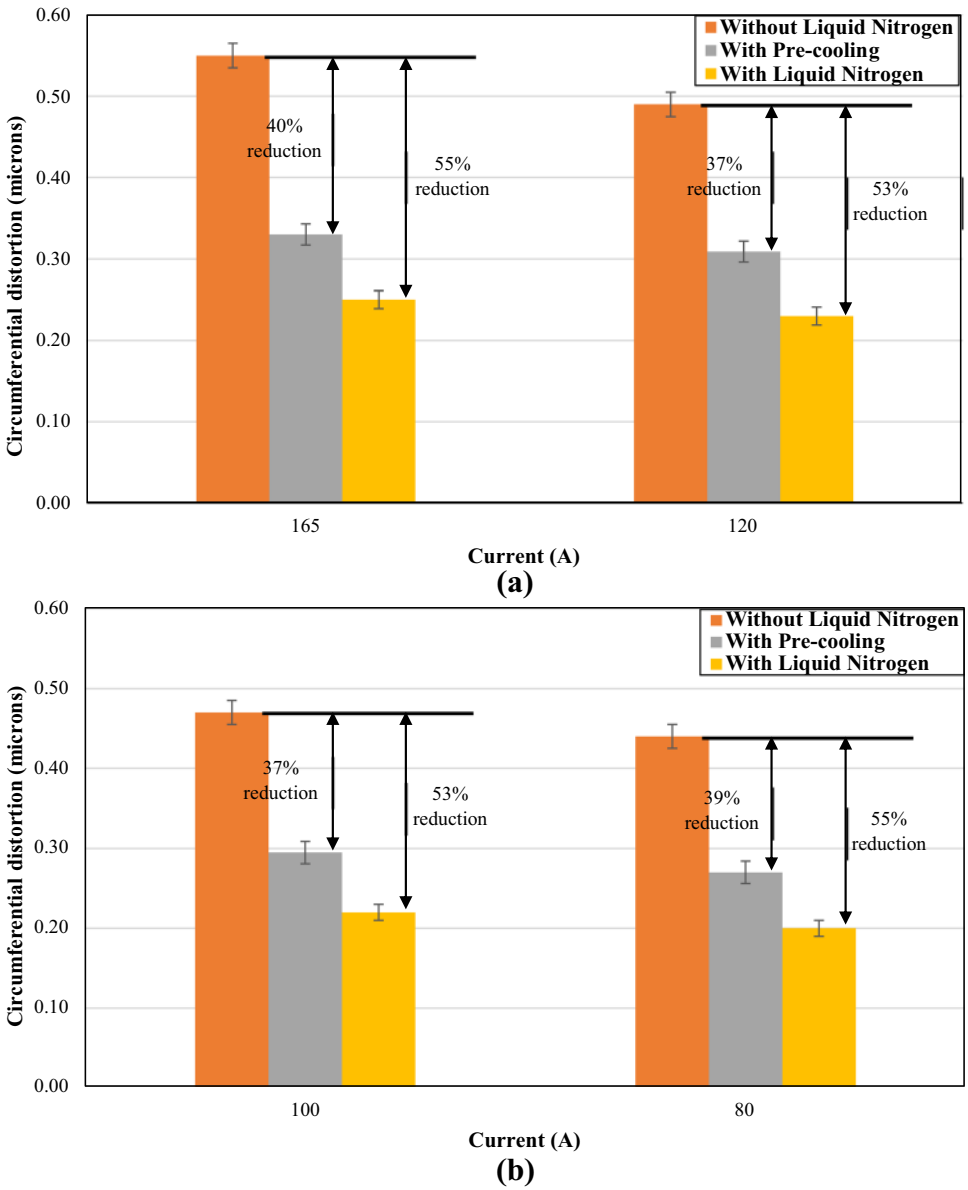

Fig. 8 Percentage reduction in circumferential distortion at the weld centerline of three groups **a** At 165 A and 120 A **b** At 100 A and 80 A

to 165 A, the percentage increase in weld penetration was more than 125%. From Fig. 10a, d it is clear that higher current resulted in high energy input [30] that melted a large quantity of metal around the vicinity of the weld. Hence, resulted in greater depth of the weld.

3.2.2 Weld penetration of the specimens with trailing heat sink

Following Fig. 11a–d belong to group B in which trailing heat sink was provided. Figure 11 also shows the same increasing trend in the weld penetration with the increase in the current but with more increase in weld penetration. Figure 11a and b showed the maximum amount of penetration in this case. In the presence of a trailing heat sink, FZ and HAZ were also reduced as summarized in Table 3. Because these two parameters depend upon the heat input, welding type and heat transfer of the heat sink. In this case, heat transfer due to the intensive cooling media is more prominent.

3.2.3 Weld penetration of the pre-cooled specimens

In this group, specimens were pre-cooled with the intensive cooling media prior to welding as shown in Fig. 12a–d. Current values were varied to check the variation in penetration of the weld. These findings clearly showed that pre-cooled specimens also resulted in deeper penetration of the weld. It is because lesser circumferential distortion makes the arc length shorter.

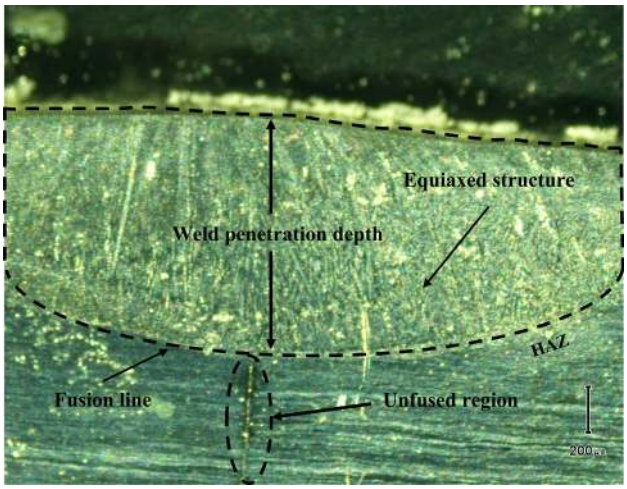

Fig. 9 Optical micrograph showing fused, unfused regions and weld penetration depth of TIG welding with cryogenic liquid

Consequently, the weld bead becomes shorter, and hence resulted in twelve percent deeper penetration as compared to autogenous TIG welding.

In all three cases, the penetration of the weld was incomplete. There are twofold reasons for this problem. Firstly, autogenous TIG welding arc as well as speed did not provide enough time to transfer the energy to the complete depth in a single pass welding. Secondly, low heat input of TIG welding as compared to conventional welding techniques can be a leading factor in influencing incomplete weld penetration. For complete penetration to take place the slow welding speed and multi-pass welding must be required.

3.3 Dependence of weld penetration on current with or without trailing heat sink

Figure 13 shows the comparison of the weld penetration of three experimental groups. It is evident from Fig. 13 that the depth of penetration increased with an increase in the current for all the cases because the increase in current resulted in an increase in temperature of the BM. This has increased the heat input per unit length of the weld bead (as presented in Table 3) that caused the melting of a large volume of the BM. Hence, resulted in deeper penetration upon the increase in current. This

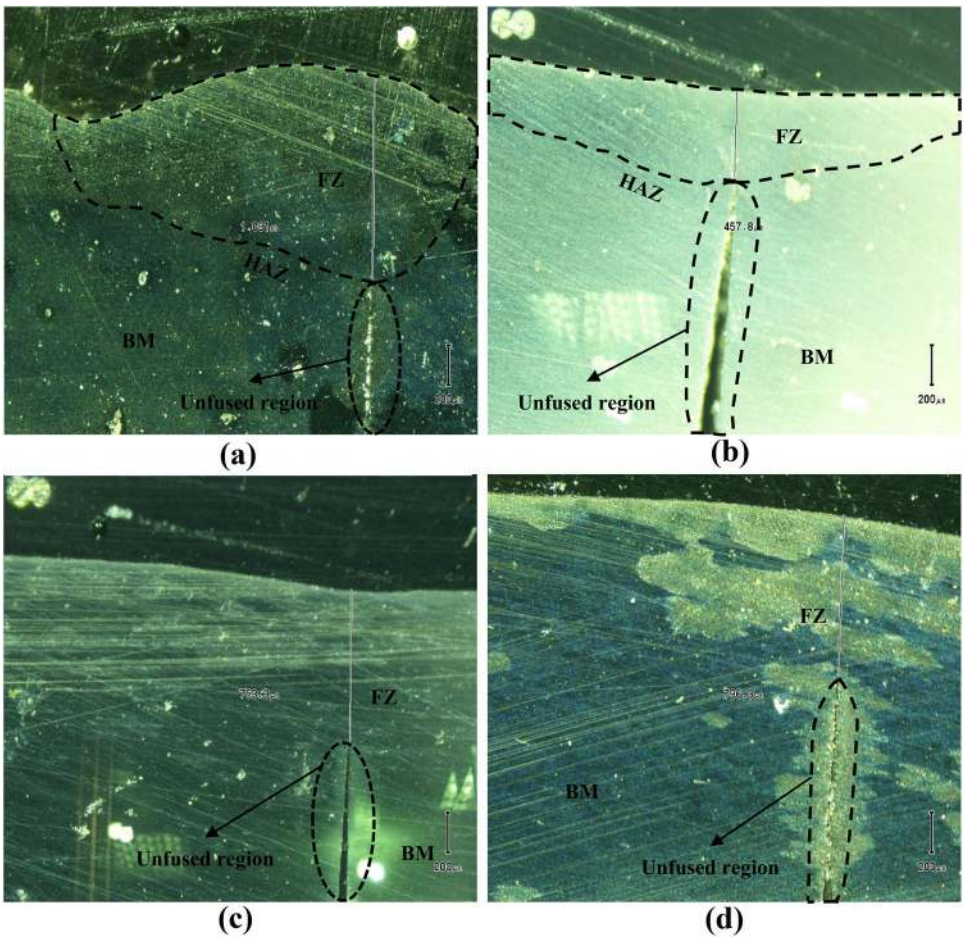

Fig. 10 Optical microscopic images of specimens showing weld penetration without cryogenic liquid **a** At 165 A, **b** At 80 A, **c** At 100 A, **d** At 120 A

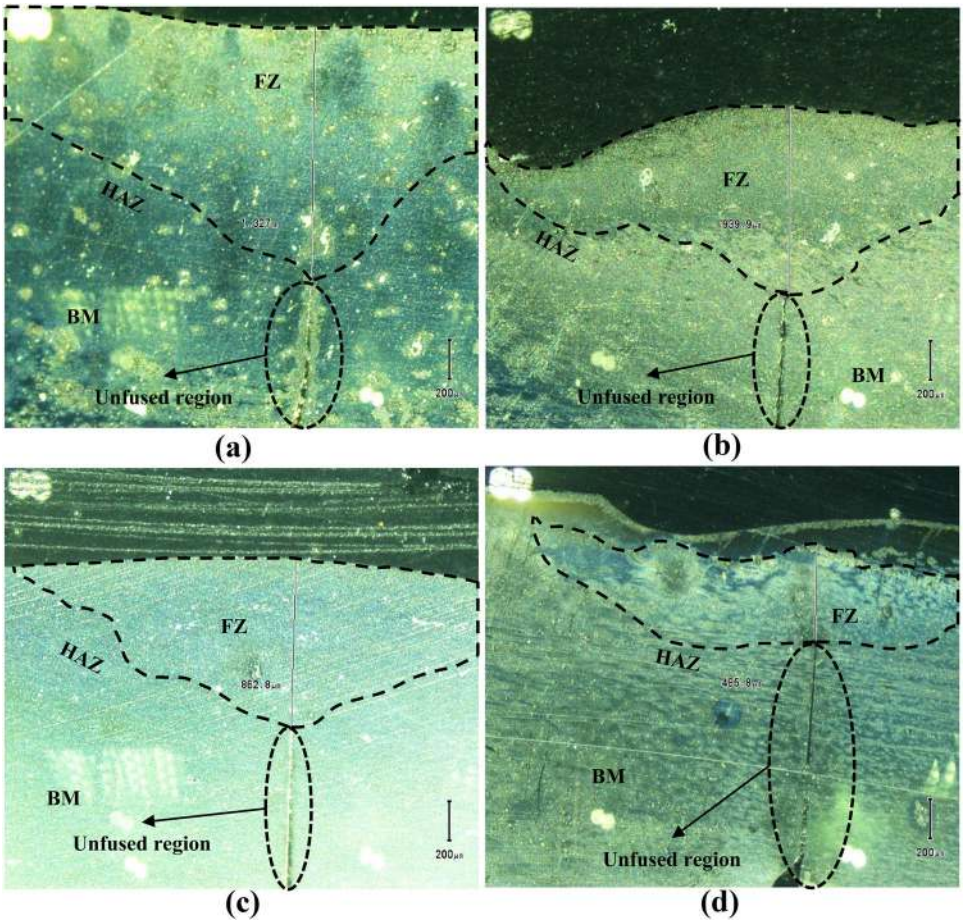

Fig. 11 Weld penetration measurement of specimens with liquid nitrogen **a** At 165 A, **b** At 120 A, **c** At 100 A, **d** At 80 A

variation of weld penetration with respect to current is consistent with the previously reported research [31]. Moreover, it is also clear from Fig. 13 that the weld is more penetrated by using the trailing heat sink as compared to the welding without trailing heat sink or pre-cooling. The length of arc plays an important part in determining the weld bead width and HAZ which affected the weld penetration, and it is more prominent in case of different cooling conditions. In the presence of tailing heat sink, the weld bead width has been minimum as shown in Fig. 7 As a result, the fused region also constricts. This is due to the reduction of peak temperature near the weld zone. All these factors resulted in the mitigation of the residual circumferential distortion. Lesser circumferential distortion mitigation would keep the arc length shorter that allows the arc to be more focused on the BM and act deeply. Consequently, there was 28% increase in the depth of weld in the presence of LN_2. In the case of pre-cooled specimens, generally more heat is necessary to increase the temperature of the specimen up to the melting point, and hence it was assumed that penetration of the pre-cooled specimen may be lower than that of ordinary TIG welding under the condition of the same heat input. But the graph shows completely opposite behavior this is due to the fact that circumferential distortion was higher with autogenous TIG welding without LN_2 as compared to pre-cooled specimens. This larger weld distortion of ordinary TIG welding as compared to pre-cooled specimens makes the arc length longer. As arc length becomes longer, the arc cone becomes broader and diverged on the BM. This makes the weld bead becomes wider as shown in Fig. 8 Consequently, TIG welding without LN_2 produces lower penetration depth than that of the pre-cooled specimen.

3.4 Dependence of weld penetration on circumferential distortion

Figure 14 depicts the variation in weld penetration as a function of residual circumferential distortion for different values of currents. Few parameters like weld width, HAZ and trailing heat sink are important for the illustration of a relationship between circumferential distortion and weld penetration. It is evident from Fig. 14 that increase in circumferential distortion resulted in a decrease of weld penetration and vice versa. This is because increased weld penetration has increased the fused region as shown in

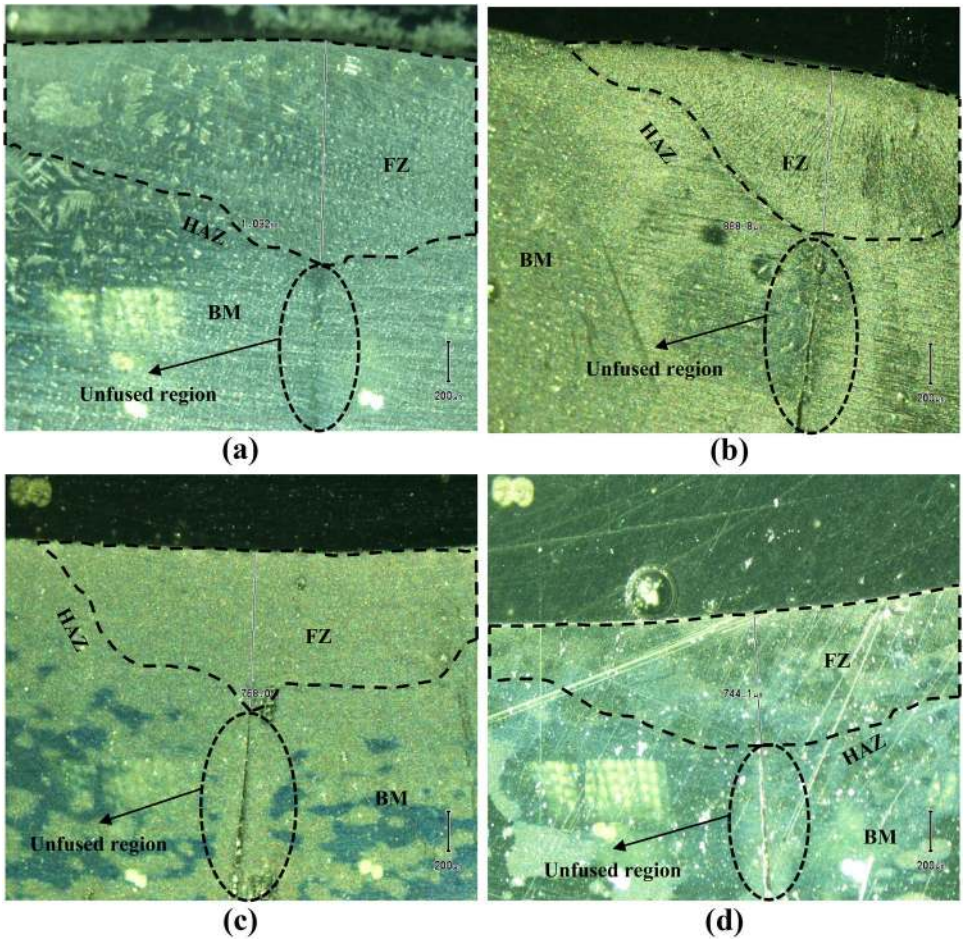

Fig. 12 Weld penetration measurement of specimens with pre-cooling **a** At 165 A, **b** At 120 A, **c** At 100 A, **d** At 80 A

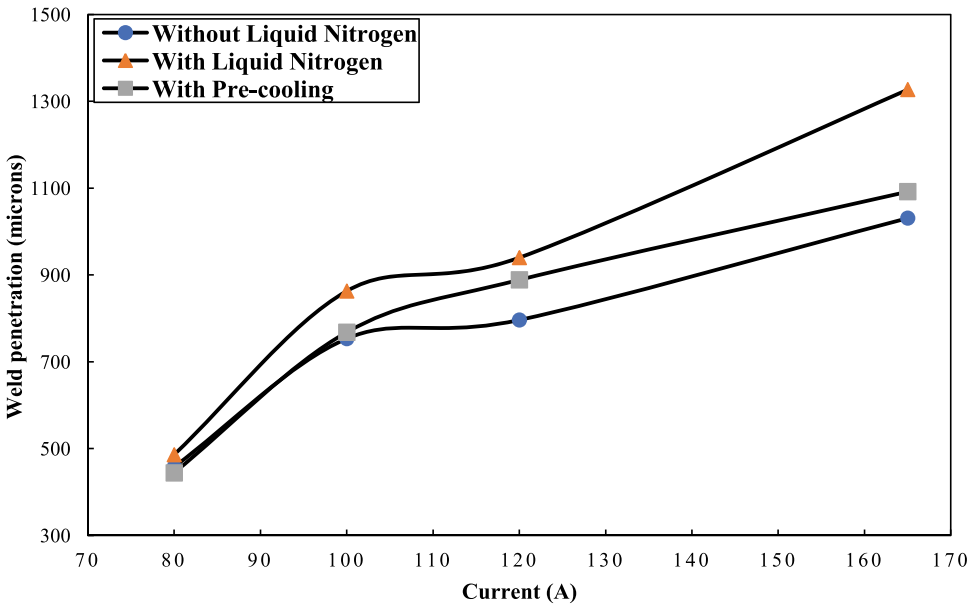

Fig. 13 Variation in weld penetration as a function of current for different groups

Fig. 9 Generally, larger FZ generates larger thermal shrinkage but in this case, the larger FZ produced lower weld circumferential distortion in the presence of a trailing heat sink. This trailing heat sink also prevents weld heat from spreading out. So the total thermal shrinkage area is limited by the trailing heat sink. Moreover, this larger FZ

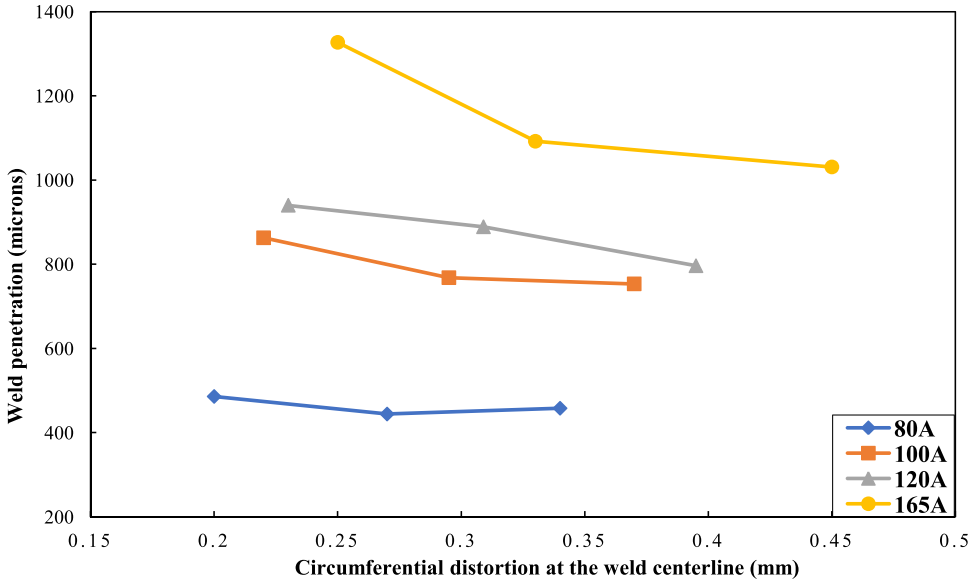

Fig. 14 Effect of circumferential distortion on weld penetration depth under different currents

produced less shrinkage due to larger melted surface area upon welding that resulted in greater conduction among the metallic structure of the specimens towards the sides of the weld bead. Consequently, the residual distortion of the welded pipe decreased. The effect of LN_2 on these two variables was more prominent for the higher value of current (165A). This relationship between these two variables is in good agreement with the observation of weld characteristics reported elsewhere [32].

3.5 Delta-ferrite distribution in the specimens with and without trailing heat sink

The study of delta-ferrite distribution across the welding zone is the prime objective of this section to evaluate the quality of welded specimens. Therefore, its local percentage is calculated at different positions of the welded specimens. A lot of literature was available on the ferrite number (FN) of welding zones, but its local percentage variance was not evaluated as a result of cryogenic TIG welding. For this purpose, a MATLAB® code for image processing was generated. This technique for the determination of delta-ferrite distribution was previously employed by one of the researchers of this paper for SMAW [33]. The distribution of delta-ferrite in different zones of TIG-welded specimens without trailing heat sink is shown in Fig. 15. The concentration of delta-ferrite was maximum at HAZ and contents suddenly decreased on both sides of HAZ as shown in Fig. 15a. It may be due to the migration of melted ferrite particles towards the heat source. The arithmetic mean of delta-ferrite acquired through this technique is compared with the value obtained through Magne-Gage tester J5-660. There was only 0.78% difference between the two techniques. Thus, a good semblance was found between these techniques. It is clear from Fig. 16 that ferrite distribution of the specimens welded using cryogenic liquid had higher contents of delta ferrite than TIG welding without intensive cooling media. Amuda et al. [34] indicated that cryogenic cooling leads to rapid dissipation of heat which would result in an equiaxed grain structure as compared to the columnar structure. Figure 9 showed that the equiaxed structure is prominent due to the presence of cryogenic liquid during welding. The shaded region in Fig. 9 showed that delta-ferrite was present in HAZ. Furthermore, rapid cooling results in less phase transformation of delta-ferrite to austenite. As a result, more concentration of delta ferrite was retained in the presence of a trailing heat sink. The ferrite contents distribution also depends upon the cooling rate and mode of solidification. LN_2 used in this experiment increased the cooling rate of the weld zone. Consequently, more delta-ferrite was retained in the weld metal after solidification. Figure 17 depicts the ferrite distribution of the samples of the welded joints pre-cooled prior to welding. Ferrite contents increased due to pre-cooling, but this increase is less significant as compared to spontaneous cooling. The findings of these results showed that delta-ferrite contents for a single pass autogenous welding were a little higher than previously reported by [35, 36]. The faster cooling rate of single-pass TIG welding in the presence of trailing heat sink resulted in retained delta-ferrite. Figures 15, 16 and 17 also depict significant increase in delta-ferrite content with an increase in current. A similar variation in delta-ferrite contents of single-pass autogenous TIG welding with respect to current was previously investigated in the researches [37, 38].

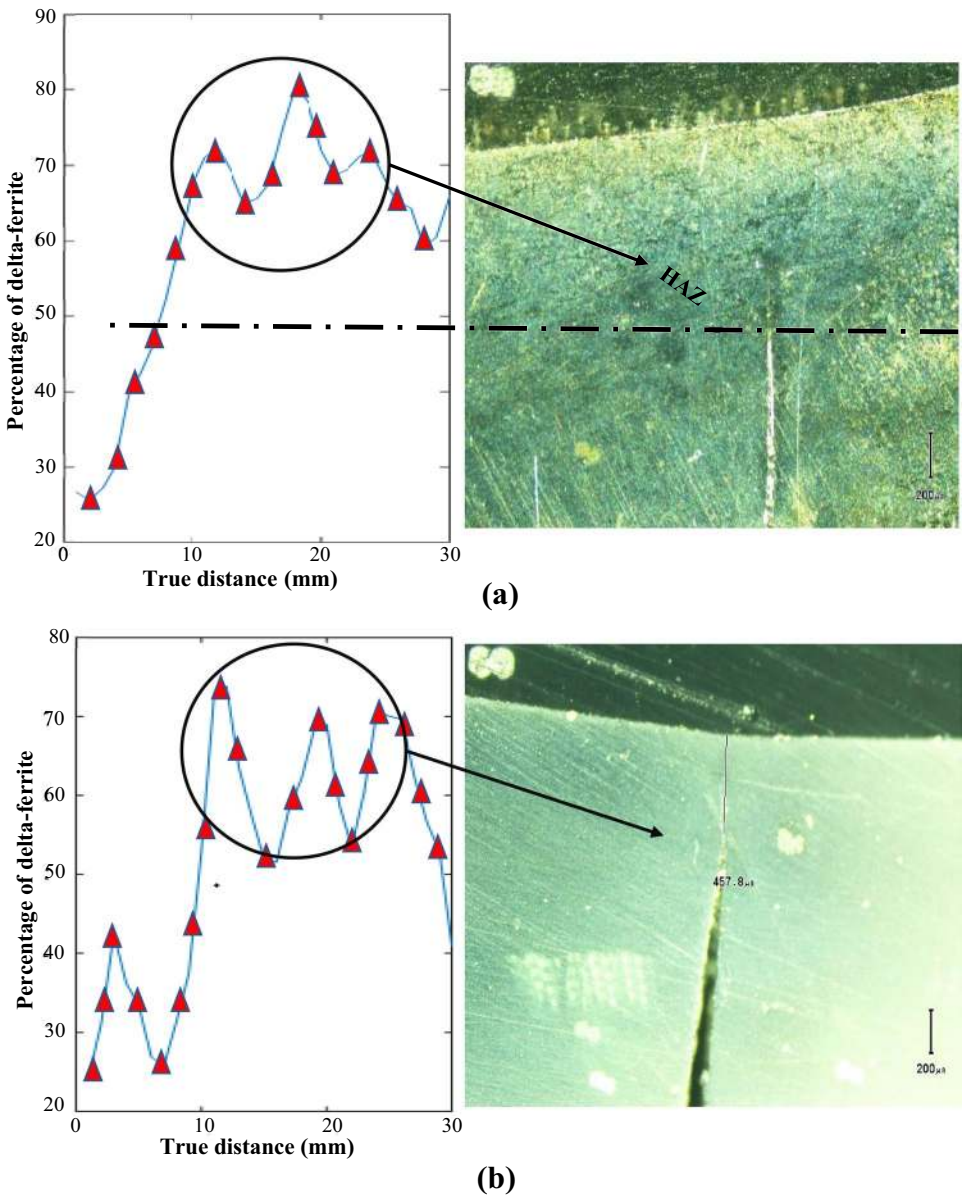

Fig. 15 Local distribution of delta-ferrite in TIG welded specimens **a** At 120 A, **b** At 80 A

4 Conclusions

In the present research, the effect of LN_2 on the circumferential distortion, microstructure, weld penetration and delta-ferrite distribution of AISI SS316 was investigated experimentally. It is found that an increase in current from 80 to 165 A resulted in a mitigation of residual circumferential distortion by 64% in the presence of LN_2 and clamping mandrel. In addition to this, weld penetration decreased with the increase in circumferential distortion and was maximum at a higher value of the current in the presence of a trailing heat sink. Moreover, cryogenic cooling of weld joints via LN_2 constricts the measured widths of the weld bead, FZ and HAZ. Furthermore, an increase in the cooling rate through the cryogenic liquid also increases the delta ferrite contents and is mostly concentrated near HAZ. Although, single-pass autogenous TIG welding in the presence of intensive

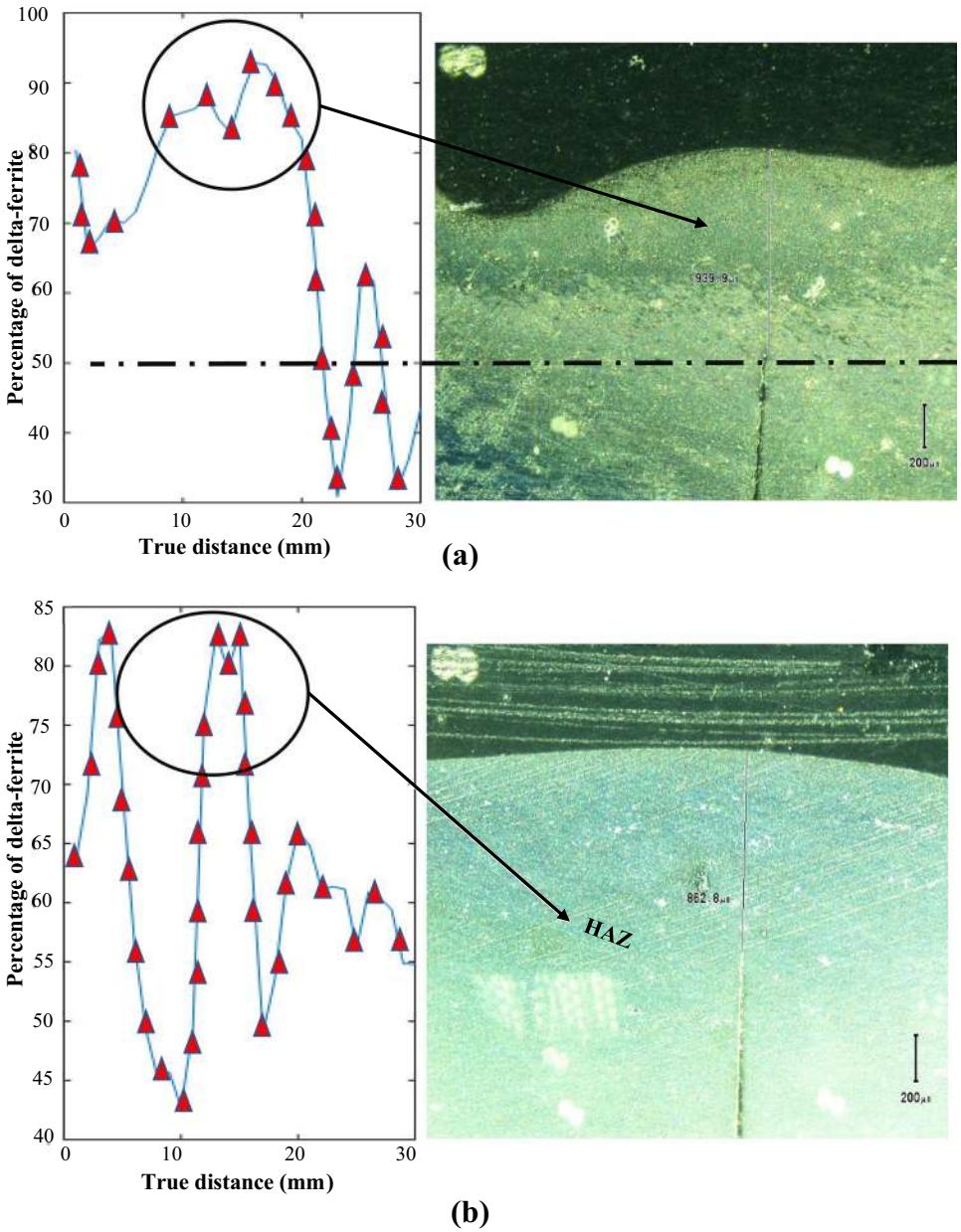

Fig. 16 Local distribution of delta-ferrite in TIG welded specimens with trailing heat sink **a** At 120 A, **b** At 100 A

cooling media didn't give complete weld penetration in this research. But it can be a suitable technique for the welding of industrial pipes to mitigate the residual circumferential distortion and increase weld penetration. Further research about multi-pass cryogenic TIG welding and slow welding speed may prove to be a pivotal factor in achieving complete weld penetration. Additionally, finite element analysis of clamped TIG-welded joints in the presence of trailing heat sink using the inherent strain method and its comparison with the experimental data acquired for the same material or different material can be considered for future researches.

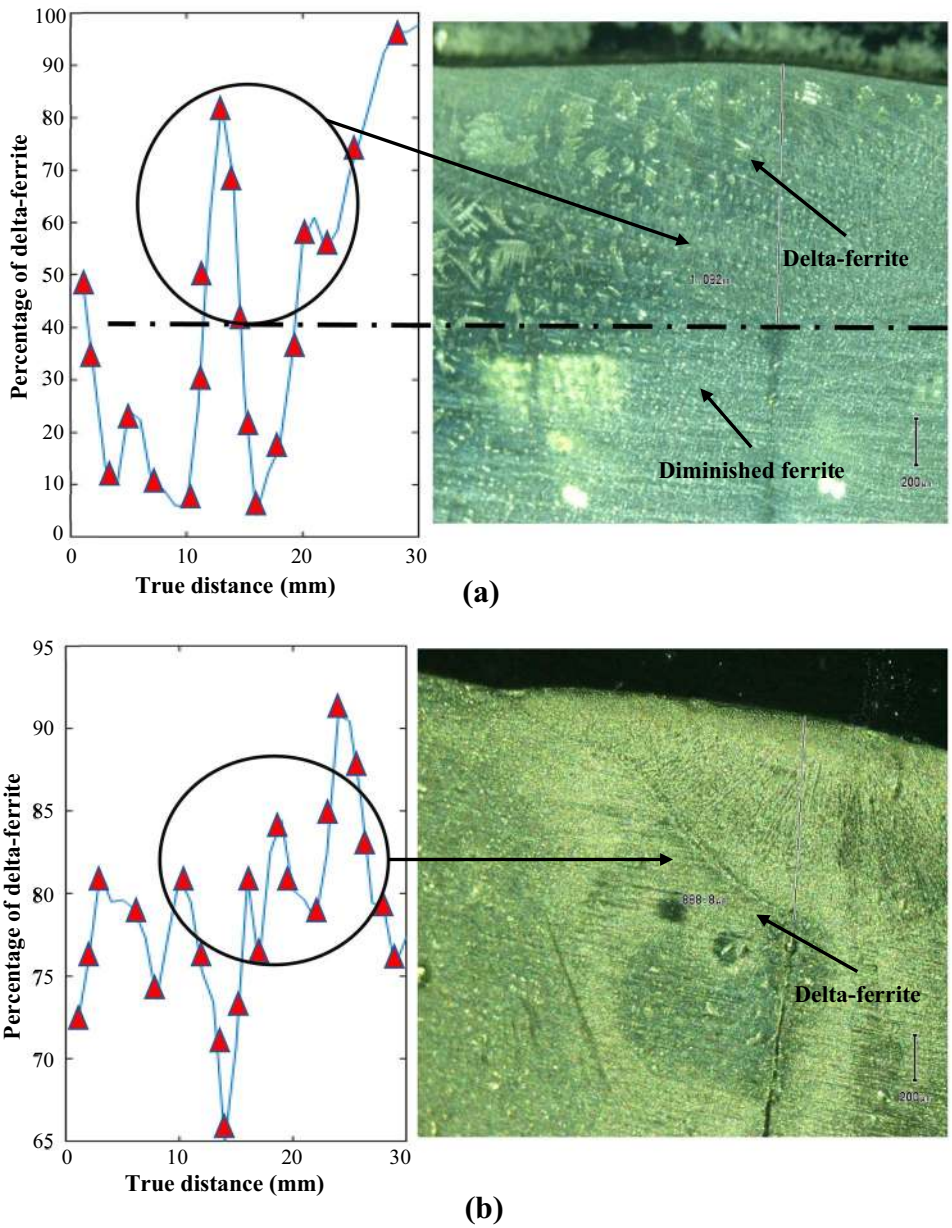

Fig. 17 Local distribution of delta-ferrite in TIG welded pre-cooled specimens **a** At 165 A, **b** At 120 A

Acknowledgements The authors acknowledge the contribution of reviewers for making this manuscript publishable by giving their valuable suggestions and comments.

Compliance with ethical standards

Conflict of interest The authors declare that they have no conflict of interest.

Availability of data and material The datasets supporting the conclusions of this article are included within the article.

References

1. Lee C-H, Chang K-H (2014) Comparative study on girth weld-induced residual stresses between austenitic and duplex stainless steel pipe welds. Appl Therm Eng 63(1):140–150. https://doi.org/10.1016/j.applthermaleng.2013.11.001
2. Pamnani R, Vasudevan M, Jayakumar T, Vasantharaja P, Ganesh K (2016) Numerical simulation and experimental validation of arc welding of DMR-249A steel. Def Technol 12(4):305–315
3. Perić M, Garašić I, Tonković Z, Vuherer T, Nižetić S, Dedić-Jandrek H (2019) Numerical prediction and experimental validation of temperature and residual stress

distributions in buried-arc welded thick plates. Int J Energy Res 43(8):3590–3600
4. Joo S-M, Kim Y-G, Jeong S-M (2017) Experimental investigation of in-process mitigation of welding distortion for stainless steel plate using air-atomized mist cooling. J Mech Sci Technol 31(9):4419–4423. https://doi.org/10.1007/s12206-017-0842-5
5. Ahn J, He E, Chen L, Wimpory R, Dear J, Davies C (2017) Prediction and measurement of residual stresses and distortions in fibre laser welded Ti-6Al-4V considering phase transformation. Mater Des 115:441–457
6. Arif ZU, Shah M, Rehman E, Tariq A (2020) Effect of spraying parameters on surface roughness, deposition efficiency, and microstructure of electric arc sprayed brass coating. Int J Adv Appl Sci 7(7):25–39
7. Ji X, Hua X, Shen C, Huang Y, Zhang Y, Cai Y (2019) Optimization of welding parameters on pores migration in Laser-GMAW of 5083 aluminum alloy based on response surface methodology. SN Appl Sci 1(10):1161
8. Islam M, Buijk A, Rais-Rohani M, Motoyama K (2015) Process parameter optimization of lap joint fillet weld based on FEM–RSM–GA integration technique. Adv Eng Softw 79:127–136
9. Altenkirch J, Steuwer A, Withers P, Williams S, Poad M, Wen S (2009) Residual stress engineering in friction stir welds by roller tensioning. Sci Technol Weld Join 14(2):185–192
10. Nam H, Park C, Kim C, Kim H, Kang N (2018) Effect of post weld heat treatment on weldability of high entropy alloy welds. Sci Technol Weld Join 23(5):420–427
11. Kumar B, Bag S (2019) Phase transformation effect in distortion and residual stress of thin-sheet laser welded Ti-alloy. Opt Lasers Eng 122:209–224
12. Guan Q, Guo D, Li C (1987) Method and apparatus for low stress and non-distortion welding of thin-walled structural elements. Chinese Patent (87100959)
13. Zhang C, Guan Q, Guo D 1996 Study on application of Dynamic control of welding stress and distortion in thin aluminium elements. In: Proc. of the 6th Int. Symp., JWS, Nagoya pp 539–544
14. Han W, Wan F, Li G, Dong C, Tong J (2011) Effect of trailing heat sink on residual stresses and welding distortion in friction stir welding Al sheets. Sci Technol Weld Join 16(5):453–458
15. Bajpei T, Chelladurai H, Ansari MZ (2016) Mitigation of residual stresses and distortions in thin aluminium alloy GMAW plates using different heat sink models. J of Manuf Process 22:199–210. https://doi.org/10.1016/j.jmapro.2016.03.011
16. Shen C (2013) Low distortion welding for shipbuilding industry.
17. Richards D, Prangnell P, Withers P, Williams S, Nagy T, Morgan S (2010) Efficacy of active cooling for controlling residual stresses in friction stir welds. Sci Technol Weld Joini 15(2):156–165
18. Xu N, Ueji R, Morisada Y, Fujii H (2014) Modification of mechanical properties of friction stir welded Cu joint by additional liquid CO2 cooling. Mater Des 1980–2015(56):20–25
19. Ji S, Yang Z, Wen Q, Yue Y, Zhang L (2018) Effect of trailing intensive cooling on residual stress and welding distortion of friction stir welded 2060 al-li alloy. High Temp Mater Process (London) 37(5):397–403
20. Tchoumi T, Peyraut F, Bolot R (2016) Influence of the welding speed on the distortion of thin stainless steel plates—numerical and experimental investigations in the framework of the food industry machines. J Mater Process Technol 229:216–229
21. Kumar N, Mukherjee M, Bandyopadhyay A (2017) Comparative study of pulsed Nd: YAG laser welding of AISI 304 and AISI 316 stainless steels. Opt Laser Technol 88:24–39
22. Aghaei A, Dehghani K (2015) Characterizations of friction stir welding of dissimilar monel400 and stainless steel 316. Int J of Adv Manuf Technol 77(1–4):573–579
23. Dhandha KH, Badheka VJ (2015) Effect of activating fluxes on weld bead morphology of P91 steel bead-on-plate welds by flux assisted tungsten inert gas welding process. J of Manuf Process 17:48–57
24. Sattari-Far I, Javadi Y (2008) Influence of welding sequence on welding distortions in pipes. Int J Press Vessels Pip 85(4):265–274
25. Prasad VV, Varghese VJ, Suresh M, Kumar DS (2016) 3D simulation of residual stress developed during TIG welding of stainless steel pipes. Procedia Technol 24:364–371
26. Wen Q, Ji S, Zhang L, Yue Y, Lv Z (2018) Temperature, stress and distortion of Ti–6Al–4V alloy low-temperature friction stir welding assisted by trailing intensive cooling. Trans Indian Inst Met 71(12):3003–3009
27. Gharib A, Biglari F, Shafaie M, Kokabi A (2019) Experimental and numerical investigation of fixture time on distortion of welded part. Int J Adv Manuf Technol 104(1–4):1121–1131
28. Li C-l, Ding F, Yu X-q, Huang J-k (2019) Residual stress and welding distortion of Al/steel butt joint by arc-assisted laser welding-brazing. Trans Nonferrous Metals Soc China 29(4):692–700
29. Sudheesh RS, Prasad NS (2015) Comparative study of heat transfer parameter estimation using inverse heat transfer models of a trailing liquid nitrogen jet in welding. Heat Transf Eng 36(2):178–185
30. Mostafa N, Khajavi M (2006) Optimization of welding parameters for weld penetration in FCAW. J achiev mat manuf eng 16(1–2):132–138
31. Zhang D-k, Yue Z, Dong M-y, Wang G-q, Wu A-p, Shan J-g, Meng D-y, Liu X-l, Song J-l, Zhang Z-p (2019) Effects of weld penetration on tensile properties of 2219 aluminum alloy TIG-welded joints. Trans Nonferrous Met Soc China 29(6):1161–1168
32. Venkatesan M, Murugan N, Prasad B, Manickavasagam A (2013) Influence of FCA welding process parameters on distortion of 409M stainless steel for rail coach building. J Iron Steel Res Int 20(1):71–78
33. Ullah M, Wu CS, Shah M (2016) In situ delta ferrite estimation and their effects on FCPR at different orientations of multipass shielded metal arc welded SS304L. J Manuf Process 21:107–123
34. Amuda M, Mridha S (2013) Grain refinement and hardness distribution in cryogenically cooled ferritic stainless steel welds. Mater Des 47:365–371
35. Batool S, Khan M, Jaffery SHI, Khan A, Mubashar A, Ali L, Khan N, Anwar MN (2016) Analysis of weld characteristics of microplasma arc welding and tungsten inert gas welding of thin stainless steel (304L) sheet. Proc Inst Mech Eng Part L J Mat Des and Appl 230(6):1005–1017
36. Tseng K-H, Hsu C-Y (2011) Performance of activated TIG process in austenitic stainless steel welds. J Mater Process Technol 211(3):503–512
37. Loureiro A, Costa B, Batista A, Rodrigues A (2009) Effect of activating flux and shielding gas on microstructure of TIG welds in austenitic stainless steel. Sci Technol Weld Joining 14(4):315–320
38. Pandey C, Mahapatra MM, Kumar P, Saini N (2018) Comparative study of autogenous tungsten inert gas welding and tungsten arc welding with filler wire for dissimilar P91 and P92 steel weld joint. Mater Sci Eng, A 712:720–737